Multiparametric approach for the evaluation of lipid nanoparticles for siRNA delivery

Citation: Alabi, C. A., K. T. Love, G. Sahay, H. Yin, K. M. Luly, R. Langer, and D. G. Anderson. "Multiparametric Approach for the Evaluation of Lipid Nanoparticles for siRNA Delivery." Proceedings of the National Academy of Sciences 110, no. 32 (July 23, 2013): 12881–12886.

As Published: http://dx.doi.org/10.1073/pnas.1306529110

Publisher: National Academy of Sciences (U.S.)

Persistent URL: http://hdl.handle.net/1721.1/89097

Version: Final published version: final published article, as it appeared in a journal, conference proceedings, or other formally published context

Multiparametric approach for the evaluation of lipid nanoparticles for siRNA delivery

Christopher A. Alabi[a,b], Kevin T. Love[a], Gaurav Sahay[a], Hao Yin[a], Kathryn M. Luly[c], Robert Langer[a,b,d,e], and Daniel G. Anderson[a,b,d,e,1]

[a]David H. Koch Institute for Integrative Cancer Research, Massachusetts Institute of Technology, Cambridge, MA 02142; [b]Department of Chemical Engineering, [d]Harvard–MIT Division of Health Sciences and Technology, and [e]Institute of Medical Engineering and Science, Massachusetts Institute of Technology, Cambridge, MA 02139; and [c]Department of Biomedical Engineering, University of Rochester, Rochester, NY 14627

Edited* by Mark E. Davis, California Institute of Technology, Pasadena, CA, and approved June 28, 2013 (received for review April 15, 2013)

Nanoparticle-mediated siRNA delivery is a complex process that requires transport across numerous extracellular and intracellular barriers. As such, the development of nanoparticles for efficient delivery would benefit from an understanding of how parameters associated with these barriers relate to the physicochemical properties of nanoparticles. Here, we use a multiparametric approach for the evaluation of lipid nanoparticles (LNPs) to identify relationships between structure, biological function, and biological activity. Our results indicate that evaluation of multiple parameters associated with barriers to delivery such as siRNA entrapment, pK_a, LNP stability, and cell uptake as a collective may serve as a useful prescreening tool for the advancement of LNPs in vivo. This multiparametric approach complements the use of in vitro efficacy results alone for prescreening and improves in vitro–in vivo translation by minimizing false negatives. For the LNPs used in this work, the evaluation of multiple parameters enabled the identification of LNP pK_a as one of the key determinants of LNP function and activity both in vitro and in vivo. It is anticipated that this type of analysis can aid in the identification of meaningful structure–function–activity relationships, improve the in vitro screening process of nanoparticles before in vivo use, and facilitate the future design of potent nanocarriers.

RNAi | thiol-yne | gene silencing | drug carrier

The successful development of siRNA therapeutics for the treatment of human diseases via gene regulation hinges on efficient delivery to the desired target site. Encapsulation of siRNAs within nanoparticles offers numerous delivery benefits, including protection from degradation by ubiquitous nucleases, passive and active targeting, and evasion of endosomal Toll-like receptors (1–3). To date, several polymeric, lipid, and dendritic nanoparticles have been developed for the encapsulation and delivery of siRNAs (4–9). Despite the delivery successes met by some of these carriers, advances are necessary to allow the fullest application of siRNA in the clinic.

Challenges to efficient delivery include nanoparticle dissociation via serum proteins (10, 11), cellular uptake (12), endosomal escape (13), and appropriate intracellular disassembly (14, 15). To address some of these challenges, single-parameter studies that evaluate the effect of chemical structure on a single biological property or on delivery performance have been carried out (16–21). Furthermore, high-throughput synthetic methods have been exploited for the accelerated discovery of potent lipid nanoparticles (LNP) and evaluation of structure activity relationships (SAR) (22, 23). Despite these efforts, the relationships between physicochemical properties of nanoparticles and biological barriers, and that between biological barriers and gene-silencing activity remain unclear. This lack of clarity is one of the reasons for poor in vitro–in vivo translation. Due to the experimental and resource limitations of in vivo experiments, many researchers rely on in vitro predictability for in vivo activity. However, the seminal work by Whitehead et al. (24) clearly demonstrates that model in vitro experiments, such as the use of in vitro nanoparticle formulations (complexes) or certain cell lines for cell culture, often fall short at screening or predicting potentially viable in vivo candidates.

Herein, we describe a systematic evaluation of multiple parameters associated with both the physicochemical properties and biological barriers to delivery for a group of LNPs. Our approach involves mapping out the entire delivery pathway and evaluating the correlation between each property or delivery barrier and gene silencing (Fig. 1*A*, steps 1–6). This systematic approach presents two potential advantages. First, the correlation of multiple physicochemical properties and biological barriers for a large set of LNPs with gene silencing allows for identification of relevant relationships between structure, biological function, and biological activity. Understanding these relationships will help improve the design of future therapeutic delivery vehicles. Second, a multiparametric evaluation with LNPs may lead to the identification of parameters that can complement in vitro gene knockdown as a prescreening tool for the selection of LNPs for in vivo use.

To obtain accurate correlations and accelerate both synthesis and evaluation, we developed a rapid and efficient two-step synthetic route for the preparation of well-defined lipids that can be formulated with siRNAs to produce LNPs. LNPs were used in this study because they have been shown to facilitate efficient delivery to hepatic and immune targets (23, 25–27). In the past few years, LNPs formulated with siRNAs against transthyretin (TTR) and proprotein convertase subtilisin/kexin type 9 (PCSK9) in rodents and nonhuman primates have produced promising preclinical results and several clinical trials involving LNPs are currently underway (28–30). Recently, clinical trials involving administration of a single dose of LNPs with siRNAs against TTR (ALN-TTR02) have shown robust knockdown of serum TTR protein levels of up to 94% (31). In addition to systemic delivery to hepatic and immune targets, LNPs have also found use in the development of improved cellular vaccine therapies for cancer treatment. LNPs formulated with siRNAs against programmed death ligands (PD-L1 and PD-L2) were recently shown to significantly boost the immunogenicity of dendritic cell-based vaccines following ex vivo treatment (32). To evaluate the potential barriers to LNP-mediated siRNA delivery, we measured (*i*) cellular uptake, (*ii*) endosomal escape capability,

Author contributions: C.A.A., R.L., and D.G.A. designed research; C.A.A., K.T.L., G.S., H.Y., and K.M.L. performed research; C.A.A., K.T.L., and D.G.A. contributed new reagents/analytic tools; C.A.A., K.T.L., G.S., H.Y., R.L., and D.G.A. analyzed data; and C.A.A. and D.G.A wrote the paper.

Conflict of interest statement: R.L. is a shareholder and member of the scientific advisory board of Alnylam. D.G.A. is a consultant with Alnylam Pharmaceuticals. R.L. and D.G.A. have sponsored research grants from Alnylam. Alnylam also has a license to certain intellectual property invented at Massachusetts Institute of Technology by R.L. and D.G.A.

*This Direct Submission article had a prearranged editor.

[1]To whom correspondence should be addressed. E-mail: dgander@mit.edu.

This article contains supporting information online at www.pnas.org/lookup/suppl/doi:10.1073/pnas.1306529110/-/DCSupplemental.

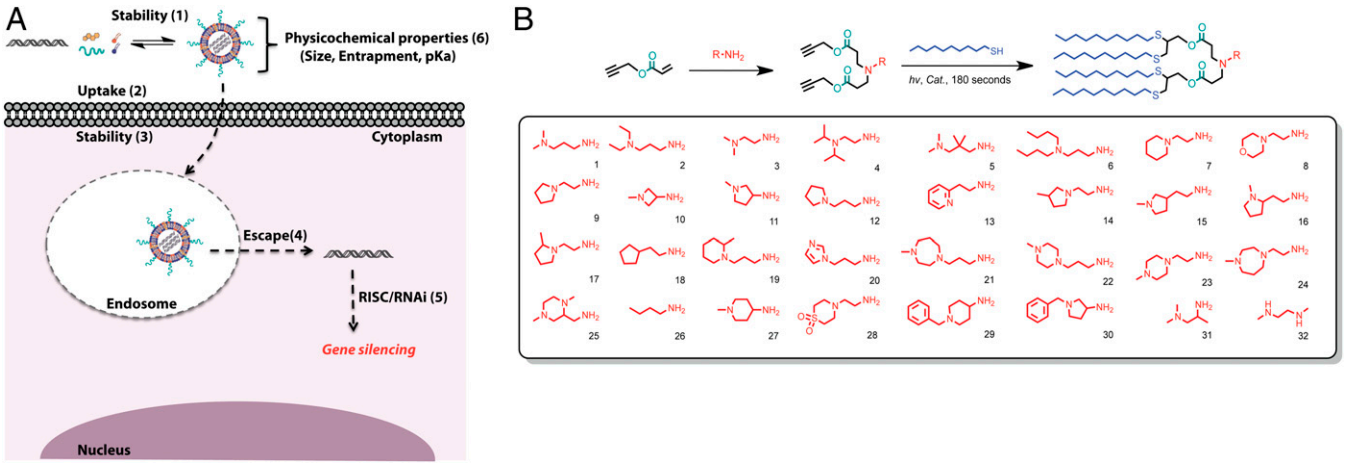

Fig. 1. (*A*) Schematic of cellular delivery pathway via LNPs. The most common barriers to delivery and the physicochemical LNP properties evaluated in this manuscript are listed in parentheses. (*B*) Synthetic scheme for the preparation of 32 unique lipidoids via the 1,4-Michael addition of a small library of primary amines (red) to propargyl acrylate followed by radical initiated thiol-yne photoaddition with 1-decanethiol. The entire lipid library was formulated into LNPs and used to evaluate correlations between gene silencing and each barrier and physicochemical property listed in *A*.

and (*iii*) extracellular and (*iv*) intracellular LNP disassembly (via FRET-labeled molecular siRNA probes) (14). All assays were adapted to a 96-well plate format, allowing for rapid throughput. Physicochemical properties of the LNPs such as size, siRNA entrapment, and pK_a were correlated with both biological barriers and gene-silencing activity.

Results

Lipid Synthesis via Thiol-Yne Chemistry. To generate meaningful relationships between structure, biological function, and biological activity, we created a diverse set of lipids for formulation with siRNAs into LNPs. Recent high-throughput screens of lipid-like materials indicate that structures with multiple short alkyl tails stemming from a polyamine core are able to facilitate efficient gene silencing (22, 23). To synthesize pure multitailed structures with varying polyamine head-group architectures, we designed a rapid and efficient two-step solvent-free synthetic route that requires neither protection/deprotection steps nor the use of costly and time-consuming chromatographic purification. The first step involves a quantitative Michael addition between a primary amine library (Fig. 1*B*) and propargyl acrylate. The resulting bis-alkyne–modified amines are subjected to a thiol-yne "click" photoaddition with decanethiol in the presence of a photocatalyst. The thiol-yne reaction is rapid and efficient and yields pure four-tailed lipid products in only 180 s after methanol precipitation (see Dataset S1 for complete characterization via MS and ^{1}H NMR). This approach generates a chemically pure library of lipids bearing the same number and position of lipid tails with differing head-group architectures. Using this two-step synthetic route, the entire purified lipid library can be generated from start to finish in parallel in less than 2 d.

In Vitro and in Vivo Gene-Silencing Evaluation of LNPs. Each member of the lipid library was formulated into LNPs with co-lipids [1,2-distearoyl-sn-glycero-3-phosphocholine (DSPC), cholesterol, and PEG-lipid] and antifirefly luciferase siRNA. HeLa cells expressing both firefly and *Renilla* luciferase genes were transfected with the LNPs in serum containing media for 24 h and assayed thereafter. *Renilla* expression was monitored as an internal control for LNP-related cytotoxicity. Transfection with LNPs in vitro resulted in a hit rate of ~40% (i.e., 40% of the lipids achieved greater than 50% gene silencing) even at siRNA doses as low as 10 ng (~7 nM siRNA concentration). None of the LNPs tested appeared toxic to cells at the doses tested (Fig. S1). After further analysis of the LNP transfection data, several SARs become apparent. We observed that structures containing aromatic (compounds **13**, **20**, **29,** and **30**) and bulky head groups (compounds **4, 6**, **21**, **24**, **29,** and **30**) as well as those with fewer than two nitrogen atoms (compounds **18** and **26**) gave poor gene silencing (Fig. S2*A*). There was no difference in performance between structures bearing acyclic head groups. However, lipids with four- to five-membered rings in their head groups (with a few exceptions) generally performed better than those with six- to seven-membered rings in their head group (Fig. S2*B*). We also observed that a subtle change in the group neighboring the ionizable amine group (compounds **9** vs. **17** vs. **14**) or a change in the position of the ionizable amine group (compounds **9** vs. **16** vs. **15**), leads to dramatic changes in gene-silencing performance (Fig. S3 *A* and *B*).

LNP performance in vivo was evaluated using a mouse murine clotting factor VII (FVII) model for monitoring hepatocyte-specific delivery (5, 22). The FVII model was primarily chosen for this evaluation because previous work from our laboratory and others have demonstrated that ionizable LNPs, similar to those prepared in this work, target liver hepatocytes presumably due to interactions with endogenous lipoproteins (25). All 32 members of the lipid library were formulated into LNPs with siRNA against FVII and administered i.v. at a dose of 1 mg/kg because this dose maximized the spread of the data. Knockdown results from these experiments showed a hit rate of ~40%, similar to the rate obtained in vitro (Fig. S4). LNPs that show better than 50% gene silencing in vivo are colored blue, and will be represented as such throughout the paper. Furthermore, correlation between these results and the in vitro transfection data (at 25 ng siRNA) has an $R^2 = 0.53$, with two false positives and three false negatives (Fig. 2*B*). The former is expected as the barriers to delivery encountered in vivo are known to be more stringent that those in vitro. The latter shows that potential in vivo hits may be discounted and never discovered. To understand the mechanism behind the uncovered SARs and in vitro–in vivo correlations, we carried out an investigation into the physicochemical properties of these LNPs as well as the barriers they need to overcome to allow for efficient delivery of the siRNA payload.

Correlations Between Biological Barriers and Gene Silencing. One of the early barriers (barrier 1 in Fig. 1*A*) encountered by nanoparticles en route to the target cell is serum protein binding and the

potential for premature nanoparticle disassembly in the extracellular milieu. As such, extracellular stability of the LNPs was measured via a recently developed FRET-labeled siRNA probe technique (14). The probe design is based on a FRET-labeled siRNA pair (Alexa Fluor 594/647) that fluoresces because of the proximity of the siRNA pair in the intact nanoparticle. A key advantage of this technique is that the lipids do not need labeling, thus allowing the entire library to be assayed and compared using the same probe conditions. LNPs formulated with the FRET-labeled siRNA pair were monitored in serum containing cell media at 37 °C for 4 h. Fig. 3*A* shows the assembly state of the LNPs (represented by the FRET signal) as a function of time. The data shows that LNPs with near-complete disassembly (i.e., FRET values near 1) after 2 h had very poor gene-silencing activities (Fig. 3*B*).

Next, LNPs that remain stable in the extracellular milieu must cross the cellular membrane barrier (barrier 2, Fig. 1*A*) to gain entry into the cell's endocytic compartment. As such, cellular uptake of LNPs containing fluorescently labeled siRNAs was measured in HeLa cells via flow cytometry. The results in Fig. 3*C* indicate that a certain uptake threshold exists below which gene silencing is not observed. These results indicate that although uptake is a critical barrier, it alone cannot guarantee efficient delivery.

LNPs must cross the cellular membrane as intact nanoparticles and resist premature dissociation at the cell membranes via surface proteoglycans (barrier 3, Fig. 1*A*) (33, 34). Because cellular uptake is strictly a measure of total cellular–associated fluorescence, LNPs that dissociate at the cell membrane or dissociated fluorophores that are nonspecifically taken up by cells may be included as part of the total cellular LNP count. To account for this non-LNP fluorescence, intact LNPs were differentiated from free siRNAs by measuring the FRET signal in HeLa cells soon after transfection with LNPs containing FRET-labeled siRNA probes. Intracellular FRET data at an early time point indicated that uptake of intact LNPs was necessary for gene silencing (Fig. 3*D*). LNPs that showed limited cellular uptake gave no intracellular FRET. However, a few LNPs with relatively high uptake such as compounds **4** and **28** (Fig. S5*A*) did not give an intracellular FRET signal (Fig. S5*B*). This result suggests that these LNPs may dissociate soon after cellular entry, thus explaining their high uptake but limited gene-silencing performance.

Following cellular uptake, it is believed that LNPs residing in the endocytic vesicles (Fig. S6) must escape this compartment (barrier 4, Fig. 1*A*) to gain access to the RNAi machinery (35, 36). The relative capacity for LNP-mediated endosomal escape was simulated using a RBC hemolysis assay. RBC hemolysis was used as a surrogate assay for endosomal escape due to similarities in their lipid bilayer (phospholipid and cholesterol) and glycocalyx compositions (37). However, we note that this model is limited in scope because the protein compositions of endosomes and RBCs do differ and endosomes do not have a membrane skeleton that is present in RBCs. This assay was performed both at a physiological pH of 7.4 and endosomal pH of 5.5 (38). Membrane lysis at pH 7.4 is an indication of toxicity, and lysis at 5.5 is a model for the ability of the LNPs to escape vesicular structures (e.g., endosomes/lysosomes) upon acidification. All LNPs tested were nonhemolytic at physiological pH (Fig. S7). However, at pH 5.5, a majority of LNPs induced varying degrees of RBC hemolysis (Fig. S7). LNPs that showed less than 10% hemolysis (after normalization to the negative control) had very poor gene-silencing activities (Fig. 3*E*). Although some LNPs appear to be hemolytic (e.g., LNPs **2** and **3**), large amounts of LNPs and siRNAs still appear to reside in the endocytic vesicles (Fig. S6, punctate dot structures in cells).

Correlations Between Physicochemical Properties, Biological Barriers, and Gene Silencing. We investigated three physicochemical properties of the LNPs including LNP size, siRNA entrapment, and pK_a. Of these three, the LNP pK_a showed the strongest correlation with biological barriers and gene silencing. LNP pK_a was measured using a well-known 2-(*p*-toluidino)-6-napthalene sulfonic acid (TNS) assay (17, 39) by titrating the LNPs from pH 2.5–8.5. The pK_a of each fully formulated LNP was determined from the resulting fluorescence titration S-curve using a curve-fit analysis. The advantage of this method is that LNP structure and formulation are taken into account and thus the measured pK_a represents that of the LNP as a whole rather than just the individual lipid (17). The measured pK_a values (Fig. S8*A*) showed good correlations with extracellular FRET and cellular uptake (Fig. 4*B*). This suggests that the charge state of the LNP has an influence on the stability and cellular uptake of LNPs. The pK_a of the LNPs also showed a nonlinear correlation with their hemolytic ability at pH 5.5 (Fig. 4*C*). LNPs with strong hemolytic ability (above 50% hemolysis) had pK_a values between 6 and 7 (Fig. 4*C*). Finally, the pK_a's of the LNPs show a nonlinear correlation with in vitro gene silencing (Fig. 4*D*). All of the top performers in vivo (above 50% silencing, color coded blue in Fig. 4*D*) have pK_a's in the range of 6–7 and all lipids with pK_a's below 5.8 (14 out of 32 lipids) were unable to silence the target gene both in vitro and in vivo. These results parallel those from a recent publication showing that an optimal pH range between 6.2 and 6.5 is required for maximum activity of ester- and dioxolane-based lipids (19).

The LNPs examined all had similar diameters as measured by dynamic light scattering (Fig. S8*B*). The siRNA entrapment for each LNP was measured via a Ribogreen exclusion assay (Fig. S8*B*) and the results indicate that compounds with low-entrapment efficiencies (under 50%) such as compounds **18**, **24,** and **26** are still able to form nanoparticles (see particle size in Fig. S8*B*), but are unable to silence the target gene.

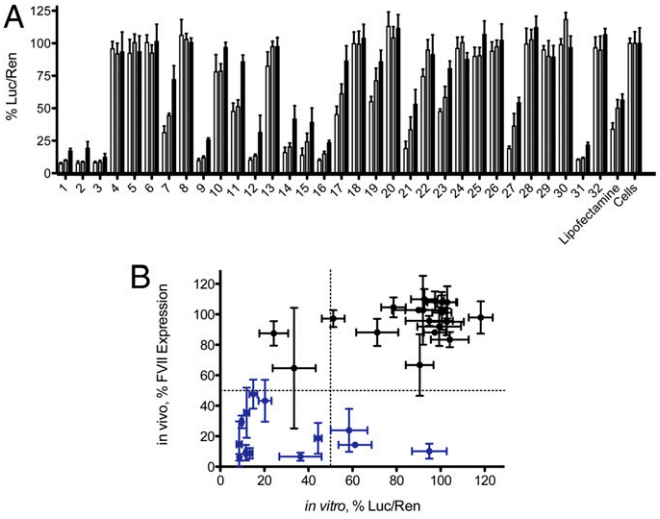

Fig. 2. (*A*) Dose-dependent knockdown of firefly luciferase via LNP-siRNA in a HeLa cell line expressing both firefly and *Renilla* luciferase. Results are presented as the luciferase expression normalized to the *Renilla* expression; (white bars) 50 ng siRNA, (gray bars) 25 ng siRNA, (black bars) 10 ng siRNA. Error bars represent SD, $n = 6$. (*B*) Correlation between in vitro luciferase (at 25 ng siRNA) and in vivo FVII gene expression. Vertical error bars represent SD, $n = 6$, horizontal error bars represent SD, $n = 3$. Dotted lines represent the 50% in vitro and in vivo gene expression levels. (*Top Left*) False positives, (*Bottom Right*) false negatives. Compounds that give better than 50% knockdown in vivo are highlighted in blue.

Discussion

To rationally design nanoparticles that can overcome the transport barriers facing delivery of siRNAs, it is necessary to understand the relationship between the physicochemical properties of the nanoparticles and the biological barriers they face. For

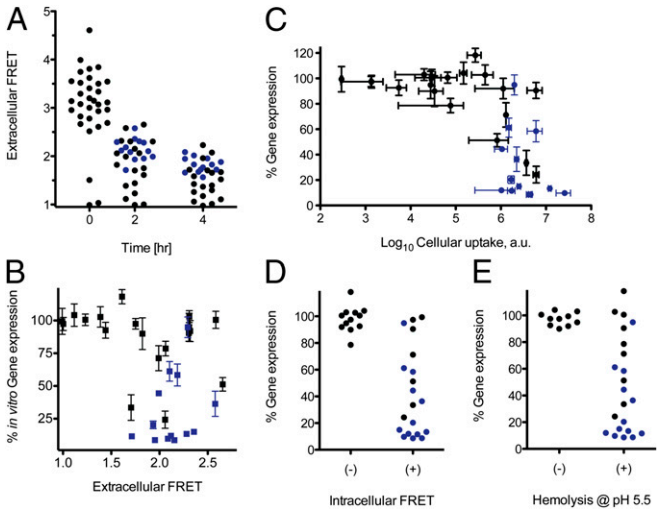

Fig. 3. LNPs that give better than 50% knockdown in vivo are highlighted in blue. (*A*) Extracellular FRET of all 32 LNPs as a function of time. (*B*) Correlation between in vitro percent of gene expression and extracellular FRET (measured after 2 h). Black vertical error bars represent SD, $n = 6$. (*C*) Correlation between in vitro percent gene expression and cell uptake. Black vertical error bars represent SD, $n = 6$. Horizontal error bars represent SD, $n = 2$. (*D*) Relationship between in vitro percent gene expression and intracellular FRET; (+) and (–) indicate the presence and absence of an intracellular FRET signal, respectively. (*E*) Relationship between in vitro percent gene expression and hemolysis at pH 5.5. (+) and (–) indicate hemolysis greater or less than 10% (after normalization to the negative control).

this reason, we set out to evaluate multiple parameters associated with the barriers to delivery and physicochemical properties of LNPs. Results from this evaluation suggest that most barriers and properties present a certain threshold below which efficient delivery is not realized. For example, LNPs showing less than 10% hemolysis were inefficient at silencing the target gene. Likewise, LNPs with pK_a values less than 5.5 were unable to silence the target gene in vitro and in vivo. We envisioned that the collective of all of the measured parameters might provide additional insight into the potential for in vivo activity beyond what is inferred from in vitro gene silencing alone. To do this, we condensed all of the measured parameters and properties into a simplified heat map and overlaid the heat map with gene-silencing performance (Fig. 5).

Each row in the heat map represents a physicochemical property or parameter associated with a cellular barrier (right *y*-axis) and the color gradient (light orange to red) represents their respective magnitude. For example, the red blocks in the first row in Fig. 5 represent high siRNA entrapment values (80–100%), and the light orange blocks represent low entrapment values (under 40%). The collective dataset in Fig. 5 indicates that LNPs capable of overcoming most of the listed barriers (greater number of red blocks) are able to silence the target gene in vivo. Prescreening based on the collective data as a metric resulted in zero false negatives and two false positives (LNPs **15** and **19**). In contrast, three false negatives (LNPs **17**, **22,** and **23**) and two false positives (LNPs **15** and **21**) were obtained using in vitro gene silencing alone as a screening parameter (cf. Figs. 2*B* and 5). As such, the collective use of all of the in vitro parameters complements the use of the in vitro transfection dataset alone for prescreening and can help reduce the occurrence of false negatives.

The evaluation of multiple physicochemical properties and biological barriers can also aid design and optimization of future LNPs through the recognition of relationships between structure, biological function, and biological activity. An example in this study involves the relationship between cellular barriers, LNP pK_a, and lipid structure. LNPs with low stability, cellular uptake, and hemolysis and subsequently low gene silencing were shown to possess low LNP pK_a's, between 3 and 6 (Fig. 4). The low LNP pK_a of some formulations can be predicted based on lipid structure. For example, lipid structures with electron-withdrawing groups neighboring the amine in the head group are weak bases (**13**, **20**, **28**, **29,** and **30**) and may thus lead to low LNP pK_a's. Other formulations were less predictable. We observed that structures with aliphatic bulky head groups (**4**, **6, 21,** and **24**) also resulted in LNP formulations with low pK_a values, which subsequently results in low gene silencing. This discovery could be used to inform the design of new lipid structures with specific head-group/tail geometries for the formulation of LNPs for siRNA delivery.

The "holy grail" for translation would be the development of computational models for the analysis and optimization of the complex pathway involved in the siRNA delivery process (i.e., *in silico*–in vitro translation). Studies involving computational analyses via mass-action kinetic and compartmental models have begun (40, 41), but are far from achieving true predictability due to the lack of reliable physicochemical and kinetic parameters. As such, the multiparameter analysis carried out in this work based on quantitative methodologies may prove useful for obtaining key parameters that can one day be used in an integrated-systems approach for the design and validation of computational methods for siRNA delivery.

This body of work highlights the importance of evaluating multiple parameters associated with both the physicochemical properties and barriers to delivery for a group of nanoparticles. For the LNPs studied in this work, correlations between their physicochemical properties and biological barriers led to the identification of LNP pK_a as a key determinant to LNP function and activity. Our results also indicate that evaluation of multiple parameters associated with barriers to delivery such as siRNA entrapment, pK_a, LNP stability, cell uptake, and hemolysis as a collective can serve as a reliable tool for prescreening LNPs before in vivo use. This multiparametric approach complements the use of in vitro results alone for prescreening and improves in vitro–in vivo translation by minimizing false negatives. Overall,

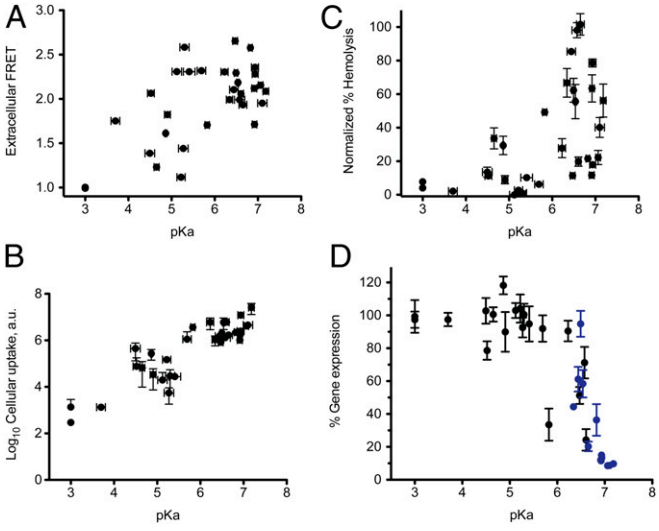

Fig. 4. (*A*) Correlation between the extracellular FRET signal after 2 h of incubation in serum containing media and LNP pKa. (*B*) Correlation between cell uptake of LNPs after 2 h incubation in serum containing media and LNP pKa. (*C*) Correlation between LNP-mediated cell hemolysis at pH 5.5 and LNP pKa. (*D*) Correlation between LNP pKa and in vitro gene expression after transfection with 25 ng siRNA. LNPs that give better than 50% knockdown in vivo are highlighted in blue. Vertical error bars represent SD, $n = 6$.

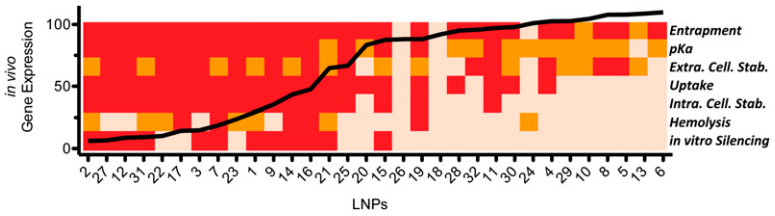

Fig. 5. A heat-map representation of the physicochemical properties and cellular functions of the LNP library from Fig. 1*B* plotted against their in vivo gene expression (black line) after administration of a 1 mg siRNA per kilogram dose. The color gradient assignment for each parameter is as follows; entrapment (light orange < 40%, orange = 40–80%, red > 80%); pKa (light orange < 4, orange = 4–6, red > 6); extracellular stability (light orange < 1.6, orange = 1.6–2.1, red > 2.1); Log_{10} uptake (red > 4.9, light orange < 4.9) au, intracellular stability (red > 0, light orange ≤ 0) au, hemolysis at pH 5.5 (light orange < 33.3%, orange = 33.3–66.7%, red > 66.7%), in vitro gene expression (red > 50%, light orange < 50%).

we anticipate that this type of multiparametric analysis on a group of nanoparticles, be it lipids, polymers, or dendrimers, may aid in the identification of relevant relationships between structure, biological function, and biological activity; improve the in vitro screening process before in vivo use; and facilitate the future design of potent nanocarriers.

Materials and Methods

A summary of experimental techniques is presented here. For full details and methods including lipid and LNP characterization, please see the *SI Materials and Methods*.

General Synthesis of Lipids. All lipids were synthesized in two steps starting from commercially available amines 1–32 (Fig. 1). The first step involves the reaction of an amine with 2.5 equivalents of propargyl acrylate neat at 45 °C overnight. Excess unreacted propargyl acrylate was removed via a centrifuge evaporator (Genavac). The corresponding pure bis-alkyne products (confirmed via ^{1}H NMR and LCMS) were combined with 5.6 equivalents decanethiol and 4% (wt/wt) 2,2-dimethoxy-2-phenylacetophenone and subsequently UV irradiated for 180 s at 10 mW/cm^2. The desired product was precipitated with methanol and dried down with a centrifuge evaporator. The final pure product was characterized via liquid chromatography–mass spectrometry (L-CMS) and ^{1}H NMR (*SI Materials and Methods*).

LNP Formulation for in Vitro and in Vivo Studies. Lipid nanoparticles were formulated by mixing an equal volume of ethanolic lipid solution with a siRNA solution in 10-mM citrate buffer at pH 3 to give a 5:1 synthesized lipid: siRNA ratio. The resulting solution was then diluted in an equal volume of 1× PBS. The ethanolic lipid solution contained a mixture of synthesized lipids, cholesterol (Sigma Aldrich), DSPC (Avanti Polar Lipids), and mPEG2000-DMG (MW 2660, a gift from Alnylam Pharmaceuticals) at a molar ratio of 50:38.5:10:1.5 in 200-proof ethanol. For all studies, the ethanolic lipid and siRNA solutions were hand mixed via pipette. The LNPs for in vivo use were also dialyzed for 75 min against 1× PBS in 3500 MWCO cassettes (Pierce/Thermo Scientific) before use.

In Vitro Transfection. In vitro transfection was performed on HeLa cells stably modified to constitutively express both firefly and *Renilla* luciferase. Cells were maintained at 37 °C in a 5% (vol/vol) CO_2 atmosphere in high-glucose Dulbelco-modified Eagles medium without phenol red (Invitrogen) supplemented with 10% (vol/vol) FBS (FBS, Invitrogen). Before transfection 15,000 cells were seeded in white 96-well plates and allowed to attach overnight. On the day of transfection, the media was replaced with 90 μL of fresh media. LNPs were formulated at a concentration of 10 ng/μL and diluted with 1× PBS to obtain the desired concentration. For example, to achieve a transfection of 25 ng of siRNA per well, the 10 ng/uL stock was diluted 1:4 to give 2.5 ng/μL, and 10 μL of this solution was added to the cells in 90 μL of media. Lipofectamine (RNAiMAX) was used according to the manufacturer's instructions as a positive control. Relative firefly luciferase silencing was assessed ∼24 h after LNP addition using a Dual-Glo luciferase assay kit (Promega). The firefly luciferase values were normalized to the *Renilla* luciferase values to correct for potential toxicity and/or off-target effects. All experiments were carried out in sextuplicates.

In Vivo FVII Gene Silencing. All animal experiments were conducted using institutionally approved protocols. C57BL/6 mice (Charles River Laboratories) were warmed under a heat lamp and weighed before receiving tail vein injections of either PBS (negative control) or LNPs containing siRNA against FVII at a dose of 1 mg/kg total siRNA. Two days postinjection, mice were anesthetized via isoflurane inhalation and ∼200 μL of blood was collected retroorbitally into microtainer tubes (BD Biosciences). Blood was centrifuged at 4000 × g for 10 min, and the supernatant was analyzed for FVII using a Biophen FVII assay kit (Aniara Corporation).

Extracellular/Intracellular FRET Assays and Cellular Uptake. LNPs containing an equimolar mixture of siRNAs labeled with Alexa Fluor594 and Alexa Fluor647 were diluted to 10 ng siRNA per microliter with 1× PBS and added to a black 96-well plate preplated with 20,000 HeLa cells at 37 °C. Control wells contained LNPs with 1% (vol/vol) Triton-X. To measure FRET, the samples were excited at 540 nm and the fluorescence intensity was read at 690 and 620 nm using a Tecan Safire^2 Microplate reader at 37 °C. FRET was determined as the ratio of the fluorescence intensities at 690/620 nm. FRET signals for all LNPs were normalized to that of the control wells. For extracellular FRET experiments, an identical experiment was carried out without cells and the FRET data obtained was similar. For intracellular FRET studies, the media was aspirated and cells were washed with calcium and magnesium free 1× PBS and trypsinized with 30 μL of 0.25% trypsin-EDTA. The trypsined cells were then neutralized with 120 μL of quenching media [25% (vol/vol) cell culture media in 1× PBS] and transferred to a 96-well v-bottom plate and analyzed via flow cytometry. For each sample, 10,000 events were monitored and evaluated by a BD LSR II HTS flow cytometer (BD Bioscience). Samples were excited with a 561-nm excitation laser and their emission was observed with a 695/40-nm emission filter set. The emission signal obtained was normalized to the emission signal obtained from the Alexa Fluor647 channel to normalize for the total LNP uptake at each time point. In addition, each channel was compensated for bleedthrough using single fluorophore controls. For cell-uptake studies, LNPs formulated with just Alexa Fluor647 were analyzed using settings for the Alexa Fluor647 channel: excitation via a 633-nm (red, HeNe) laser and emission via a 660/20-nm filter.

Hemolysis Assay. Human RBCs (Innovative Research) were washed twice with 1× PBS and diluted in either 1× PBS or citrate buffer saline at pH 5.5 (CBS, 20 mM citrate buffer, 130 mM NaCl) to a 4% vol/vol RBC solution. In a v-bottom 96-well plate, 100 μL of blank LNPs formulated at an equivalent concentration of 23.75 ng siRNA/μL (however, no siRNA was used) were added to 100 μL of the 4% vol/vol RBC solution in either PBS or CBS and heated to 37 °C for 1 h. After cooling, the plate was centrifuged at 4 °C at 1,000 × g for 5 min; 100 μL of the supernatant was transferred into a clear 96-well assay plate and the UV absorption was read 540 nm. Positive and negative control experiments were carried out with 0.1% Triton-X (100%) and buffer alone respectively.

ACKNOWLEDGMENTS. C.A.A. thanks K. Whitehead and A. Vegas for their helpful discussions and feedback on the manuscript. The authors thank Koch Institute Flow Cytometry Core at Massachusetts Institute of Technology for their high-throughput flow cytometer and Alnylam Pharmaceuticals for their automated spinning disk confocal microscope (OPERA, Perkin Elmer). The authors also thank the National Institutes of Health (NIH) (Grant R37-EB000244) for research funding and Alnylam Pharmaceuticals for chemical and biological reagents. C.A.A. thanks the NIH for his Postdoctoral Fellowship.

1. Whitehead KA, Langer R, Anderson DG (2009) Knocking down barriers: Advances in siRNA delivery. *Nat Rev Drug Discov* 8(2):129–138.
2. Kumari A, Kumar V, Yadav SK (2011) Nanocarriers: A tool to overcome biological barriers in siRNA delivery. *Expert Opin Biol Ther* 11(10):1327–1339.
3. Wang J, Lu Z, Wientjes MG, Au JL-S (2010) Delivery of siRNA therapeutics: Barriers and carriers. *Am Assoc Pharm Sci J* 12(4):492–503.
4. Davis ME (2009) The first targeted delivery of siRNA in humans via a self-assembling, cyclodextrin polymer-based nanoparticle: From concept to clinic. *Mol Pharm* 6(3):659–668.
5. Akinc A, et al. (2009) Development of lipidoid-siRNA formulations for systemic delivery to the liver. *Mol Ther* 17(5):872–879.
6. Santel A, et al. (2006) A novel siRNA-lipoplex technology for RNA interference in the mouse vascular endothelium. *Gene Ther* 13(16):1222–1234.

7. Rozema DB, et al. (2007) Dynamic PolyConjugates for targeted in vivo delivery of siRNA to hepatocytes. *Proc Natl Acad Sci USA* 104(32):12982–12987.
8. Tang Y, et al. (2012) Efficient in vitro siRNA delivery and intramuscular gene silencing using PEG-modified PAMAM dendrimers. *Mol Pharm* 9(6):1812–1821.
9. Alabi C, Vegas A, Anderson D (2012) Attacking the genome: Emerging siRNA nanocarriers from concept to clinic. *Curr Opin Pharmacol* 12(4):427–433.
10. Merkel OM, et al. (2009) Stability of siRNA polyplexes from poly(ethylenimine) and poly(ethylenimine)-g-poly(ethylene glycol) under in vivo conditions: Effects on pharmacokinetics and biodistribution measured by Fluorescence Fluctuation Spectroscopy and Single Photon Emission Computed Tomography (SPECT) imaging. *J Control Release* 138(2):148–159.
11. Buyens K, et al. (2008) A fast and sensitive method for measuring the integrity of siRNA-carrier complexes in full human serum. *J Control Release* 126(1):67–76.
12. Mescalchin A, et al. (2007) Cellular uptake and intracellular release are major obstacles to the therapeutic application of siRNA: Novel options by phosphorothioate-stimulated delivery. *Expert Opin Biol Ther* 7(10):1531–1538.
13. Dominska M, Dykxhoorn DM (2010) Breaking down the barriers: siRNA delivery and endosome escape. *J Cell Sci* 123(Pt 8):1183–1189.
14. Alabi CA, et al. (2012) FRET-labeled siRNA probes for tracking assembly and disassembly of siRNA nanocomplexes. *ACS Nano* 6(7):6133–6141.
15. Kwon YJ (2012) Before and after endosomal escape: Roles of stimuli-converting siRNA/polymer interactions in determining gene silencing efficiency. *Acc Chem Res* 45(7):1077–1088.
16. Zhang J, Fan H, Levorse DA, Crocker LS (2011) Interaction of cholesterol-conjugated ionizable amino lipids with biomembranes: Lipid polymorphism, structure-activity relationship, and implications for siRNA delivery. *Langmuir* 27(15):9473–9483.
17. Zhang J, Fan H, Levorse DA, Crocker LS (2011) Ionization behavior of amino lipids for siRNA delivery: Determination of ionization constants, SAR, and the impact of lipid pKa on cationic lipid-biomembrane interactions. *Langmuir* 27(5):1907–1914.
18. Philipp A, Zhao X, Tarcha P, Wagner E, Zintchenko A (2009) Hydrophobically modified oligoethylenimines as highly efficient transfection agents for siRNA delivery. *Bioconjug Chem* 20(11):2055–2061.
19. Jayaraman M, et al. (2012) Maximizing the potency of siRNA lipid nanoparticles for hepatic gene silencing in vivo. *Angew Chem Int Ed Engl* 51(34):8529–8533.
20. Heyes J, Palmer L, Bremner K, MacLachlan I (2005) Cationic lipid saturation influences intracellular delivery of encapsulated nucleic acids. *J Control Release* 107(2):276–287.
21. Gratton SEA, et al. (2008) The effect of particle design on cellular internalization pathways. *Proc Natl Acad Sci USA* 105(33):11613–11618.
22. Akinc A, et al. (2008) A combinatorial library of lipid-like materials for delivery of RNAi therapeutics. *Nat Biotechnol* 26(5):561–569.
23. Love KT, et al. (2010) Lipid-like materials for low-dose, in vivo gene silencing. *Proc Natl Acad Sci USA* 107(5):1864–1869.
24. Whitehead KA, et al. (2012) In vitro-in vivo translation of lipid nanoparticles for hepatocellular siRNA delivery. *Am Chem Soc Nano* 6(8):6922–6929.
25. Akinc A, et al. (2010) Targeted delivery of RNAi therapeutics with endogenous and exogenous ligand-based mechanisms. *Mol Ther* 18(7):1357–1364.
26. Leuschner F, et al. (2011) Therapeutic siRNA silencing in inflammatory monocytes in mice. *Nat Biotechnol* 29(11):1005–1010.
27. Novobrantseva TI, et al. (2012) Systemic RNAi-mediated Gene Silencing in Nonhuman Primate and Rodent Myeloid Cells. *Mol Ther Nucleic Acids* 1:e4.
28. Semple SC, et al. (2010) Rational design of cationic lipids for siRNA delivery. *Nat Biotechnol* 28(2):172–176.
29. Fitzgerald K et al. (2012) *Phase I safety, pharmacokinetic and pharmacodynamic results for ALN-PCS: A novel RNAi therapeutic for the treatment of hypercholesterolemia* (Alnylam Pharmaceuticals, Cambridge, MA). Available at http://www.alnylam.com/capella/wp-content/uploads/2012/04/ALN-PCS-PhaseI-ATVB-April20-2012.pdf. Accessed September 8, 2012.
30. Alnylam Pharmaceuticals (2011) *Trial to evaluate safety and tolerability of ALN-PCS02 in subjects with elevated LDL-cholesterol (LDL-C).* (Registry of Federally and Privately Supported Clinical Trials, US National Institutes of Health, Bethesda). Available at http://clinicaltrials.gov/ct2/show/NCT01437059. Accessed July 15, 2013.
31. Alnylam Pharmaceuticals (2012) Trial to evaluate safety, tolerability, and pharmacokinetics of ALN-TTR02 in healthy volunteer subjects. (Registry of Federally and Privately Supported Clinical Trials, US National Institutes of Health, Bethesda). Available at http://clinicaltrials.gov/show/NCT01559077. Accessed July 15, 2013.
32. Hobo W, et al. (2013) Improving dendritic cell vaccine immunogenicity by silencing PD-1 ligands using siRNA-lipid nanoparticles combined with antigen mRNA electroporation. *Cancer Immunol Immunother* 62(2):285–297.
33. Ruponen M, et al. (2001) Extracellular glycosaminoglycans modify cellular trafficking of lipoplexes and polyplexes. *J Biol Chem* 276(36):33875–33880.
34. Ruponen M, Honkakoski P, Tammi M, Urtti A (2004) Cell-surface glycosaminoglycans inhibit cation-mediated gene transfer. *J Gene Med* 6(4):405–414.
35. Nguyen J, Szoka FC (2012) Nucleic acid delivery: The missing pieces of the puzzle? *Acc Chem Res* 45(7):1153–1162.
36. Varkouhi AK, Scholte M, Storm G, Haisma HJ (2011) Endosomal escape pathways for delivery of biologicals. *J Control Release* 151(3):220–228.
37. Evans WH, Hardison WG (1985) Phospholipid, cholesterol, polypeptide and glycoprotein composition of hepatic endosome subfractions. *Biochem J* 232(1):33–36.
38. Demaurex N (2002) pH Homeostasis of cellular organelles. *News Physiol Sci* 17:1–5.
39. Bailey AL, Cullis PR (1994) Modulation of membrane fusion by asymmetric transbilayer distributions of amino lipids. *Biochemistry* 33(42):12573–12580.
40. Varga CM, Hong K, Lauffenburger DA (2001) Quantitative analysis of synthetic gene delivery vector design properties. *Mol Ther* 4(5):438–446.
41. Bartlett DW, Davis ME (2006) Insights into the kinetics of siRNA-mediated gene silencing from live-cell and live-animal bioluminescent imaging. *Nucleic Acids Res* 34(1):322–333.